Journal of Solid Mechanics and Materials Engineering

Vol. 4, No. 8, 2010

Transient Analysis of Functionally Graded Thick Hollow Circular Cylinders under Mechanical Loadings*

Masoud TAHANI**, Taha TALEBIAN** and Akira TODOROKI***

** Department of Mechanical Engineering, Faculty of Engineering, Ferdowsi University of Mashhad, Mashhad, Iran

E-mail: mtahani@ferdowsi.um.ac.ir

*** Tokyo Institute of Technology, 2-12-1 O-okayama, Meguro, Tokyo 152-8552, Japan

Abstract

This article presents the analysis of functionally graded hollow circular cylinders with finite length under axisymmetric dynamic loads. It is assumed that the functionally graded cylinder is comprised of metal-phase and ceramic-phase whereas material properties are graded in the thickness direction of the cylinder according to power law distribution. Two-dimensional finite element method in conjunction with the Newmark method is used to solve the system of time-dependent coupled equations that govern the dynamic responses. By introducing especial elements, it is possible to distribute the material properties through the thickness of cylinder exactly according to the power law distribution. Dynamic loads applied on the cylinder are axisymmetric in the hoop direction and can vary in the radial and axial directions. As examples, the transient responses of functionally graded cylinders which are excited in radial direction by increasingly and suddenly internal pressure and line load are calculated, and the characteristics of waves are discussed. The results in the present study are obtained for thick cylinder and cylindrical shell and compared with the results for isotropic cylinders.

Key words: Functionally Graded Cylinder, Dynamic Loading, Finite Element Method, Newmark Method, Dynamic Load Factor

1. Introduction

A functionally graded material (FGM) is usually a combination of two material phases that has a gradual transition from one material at one surface to another material at the opposite surface. This transition allows the creation of multiple properties (or functions) without any mechanically weak junction or interface. Furthermore, the gradual change of properties can be tailored to different applications and service environments. It is possible with these materials to obtain a combination of properties that cannot be achieved in conventional monolithic materials. For example, thermal protection plate structures made of a two-phase ceramic/metal functionally graded composite provide heat and corrosion resistance on the ceramic-rich surface while maintaining the structural strength and stiffness by the metal-rich surface. Moreover, FGMs allow for especial optimization by grading the volume fractions of two or more constituents to improve the response of structures. If properly designed, FGMs can offer various advantages such as reduction of thermal stresses, minimization of stress concentration or intensity factors and attenuation of stress

*Received 16 Nov., 2009 (No. e156-2)
[DOI: 10.1299/jmmp.4.1223]

waves. Hence, FGMs have gained potential applications in a wide variety of engineering components or systems which include the rocking motor casing, armor plating, heat-engine components, packaging encapsulates, thermoelectric generators and human implants, just to name a few.

Some research has been done related to response of functionally graded cylinders under dynamic mechanical loads. By using Reddy's third-order shear deformation theory (without incorporating transverse normal deformation), an analytical solution was presented to predict the transient response of simply supported FGM cylindrical shells subjected to low-velocity impact by a solid striker [1]. Han et al. [2] presented a numerical method for analyzing transient waves in FGM cylinders. In their method, the FGM shell was divided into layer elements with three nodal lines along the wall thickness. The material properties within each element were assumed to vary linearly in the thickness direction. After that a solution for guided waves in graded cylinders making use of Nelson's numerical–analytical method[3] was introduced by Han et al. [4]. Also, Fourier transformation and modal analysis were employed to propose a numerical method for analyzing transient waves in FGM cylindrical shells excited by impact point loads [5]. In addition, Elmaimouni [6], using the Legendre polynomials and harmonic functions, developed a numerical method for calculating guided wave propagation in a FGM infinite cylinder. Next, vibration and radial wave propagation in FGM thick hollow cylinders were studied with assumption that the FGM cylinder was made from many isotropic subcylinders [7]. Material properties in each layer were constant and functionally graded properties were resulted by suitable arrangement of layers in the multilayer cylinder. Afterward, a thick hollow cylinder with finite length made of two-dimensional functionally graded material (2D-FGM) subjected to impact internal pressure was considered and investigated the time histories of displacements, stresses and two-dimensional wave propagation [8].

A number of works has been made related to free vibrations of functionally graded cylinders. The vibration behavior of functionally graded cylindrical shells were investigated based on Love's theory and the Rayleigh–Ritz method by Loy et al. [9] and Pradhan et al. [10]. The studies revealed that the frequency characteristics of functionally graded cylindrical shells are similar to those of isotropic shells. Yang and Shen [11] used Reddy's higher-order shear deformation shell theory to investigate free vibration and dynamic instability of functionally graded cylindrical panels subjected to thermo-mechanical loads consisting of a steady temperature change as well as static and periodically pulsating forces in axial direction. Next, the vibration of thin cylindrical shells with ring supports made of a functionally gradient material composed of stainless steel and nickel was performed by Najafizadeh and Isvandzibaei [12]. After that, a general analytical approach was presented to investigate vibrational behavior of functionally graded shells by Ansari and Darvizeh [13].

Some investigations have been done related to stabilities and buckling of functionally graded cylinders. Stability of functionally graded cylindrical and conical shells under non-periodic impulsive loading were investigated by Sofiyev [14][15]. Moreover, He [16] studied the stability of cylindrical shells composed of FGM subjected to axial compressive load. Next, Kadoli and Ganesen [17] presented linear thermal buckling and free vibration analyses of functionally graded cylindrical shells with clamped–clamped boundary conditions based on temperature-dependent material properties.

In the aforementioned works, multi-layered method has been used widely, in which a FGM cylinder is divided into several layers and each layer is divided into a number of 2-node elements along the radial direction (e.g., N elements and $N + 1$ nodes). Also, the mechanical properties have been considered to be constant inside each of elements. In the present study, by introducing especial elements in which mechanical properties can be considered variable, it is possible to distribute the material properties through the thickness of cylinder exactly according to a power law distribution. Functionally graded hollow

cylinders with finite length under axisymmetric dynamic loads are considered. The dynamic loads applied on the cylinder are axisymmetric in the hoop direction and can vary in the radial and axial directions. The governing equations of motion are solved by the two-dimensional finite element and Newmark methods.

Nomenclature

a : width of element
b : length of element
E : Young's modulus
h : thickness of cylinder
L : length of cylinder
l : normal vector
$[C]$: stiffness matrix
$\{F\}$: elements force matrix
$[K]$: elements stiffness matrix
$[M]$: elements mass matrix
n : power law exponent
P : generic material property
P_0 : value of the final load
T: time duration of sine function
t : time
u : displacement component
V : volume fraction
w : weight function
r : coordinate in thickness direction
z : coordinate in axial direction
θ : coordinate in circumferential direction
γ : angular strain
ε : normal strain
ν : Poisson's ratio
ρ : Density
σ : Stress
τ : force traction
ψ : interpolation function

Subscripts

e: local parameter
in: inner surface
out: outer surface
m : middle radius
r: radial direction
z: axial direction
θ: circumferential direction
c: ceramic
wa: incident wavelet

2. Theoretical Formulation

2.1 Material Properties of Functionally Graded Cylinders

Consider a FGM circular hollow cylinder, which is made of a mixture of ceramic and

metal with an inner radius r_{in} and an outer radius r_{out} , as shown in Fig. 1. The outer surface of the cylinder is metal-rich whereas the inner surface is ceramic-rich and material properties are graded in the thickness direction of the cylinder according to the subsequent relation:

$$P = P_{out}V_{out} + P_{in}V_{in} \tag{1}$$

where P denotes a generic material property like modulus and P_{in} and P_{out} denote the material properties of the inner and outer surfaces of the cylinder, respectively. Also V_{in} and V_{out} indicate the volume fractions of the inner and outer surfaces material, respectively. The volume fractions are consistent with the following power law distributions:

$$V_{out} = \left(\frac{r - r_{in}}{r_{out} - r_{in}}\right)^n \qquad V_{in} = 1 - V_{out} \tag{2}$$

where power law exponent n represents the material variation profile through the cylinder thickness, which is always greater than or equal to zero, and may be varied to obtain the optimum distribution of the constituent materials. The value of n being equal to zero represents a cylinder fully made of outer surface material and infinity represents a cylinder fully made of inner surface material. Fig. 2 shows the variation of volume fraction of outer surface material in the thickness direction of the FGM cylinder.

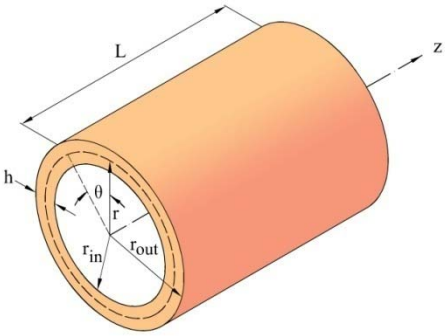

Figure 1. Schematic sketch of the cylinder and the location of coordinate system.

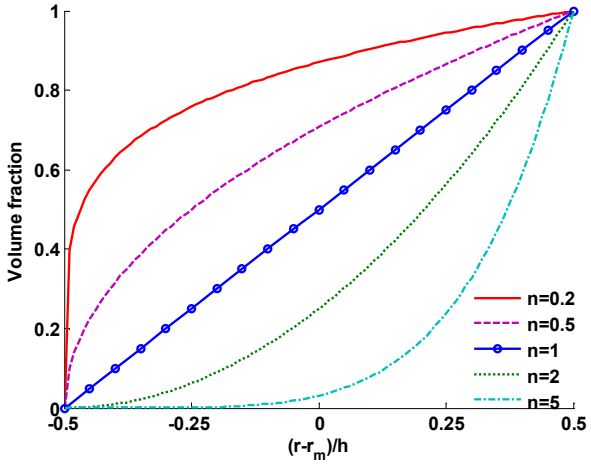

Figure 2. Variation of volume fraction of outer surface material in the thickness direction of the FGM cylinder.

2.2 Equations of Motion

As it is pointed out, it is intended here to analyze a functionally graded cylinder with finite length and subjected to axisymmetric loads. The geometry of the cylinder is shown in

Fig. 1. A cylindrical coordinate system is introduced with the origin located at the center of one end of the cylinder and coordinates r, θ and z are in the thickness, circumferential and axial directions, respectively (see Fig. 1). Since the geometry of the cylinder and the loads are assumed to be independent of the circumferential direction, the problem is axisymmetric. The governing equations of motion for this case are [18]:

$$\begin{aligned}&\frac{1}{r}\frac{\partial(r\sigma_r)}{\partial r}-\frac{\sigma_\theta}{r}+\frac{\partial\sigma_{rz}}{\partial z}=\rho\frac{\partial^2 u_r}{\partial t^2}\\&\frac{1}{r}\frac{\partial(r\sigma_{rz})}{\partial r}+\frac{\partial\sigma_z}{\partial z}=\rho\frac{\partial^2 u_z}{\partial t^2}\end{aligned}\tag{3}$$

where u_z and u_r denote the displacement components in the axial and radial directions, respectively. Also, the strain-displacement relations are [18]:

$$\varepsilon_r=\frac{\partial u_r}{\partial r},\quad \varepsilon_\theta=\frac{u_r}{r},\quad \varepsilon_z=\frac{\partial u_z}{\partial z},\quad \gamma_{rz}=\frac{\partial u_r}{\partial z}+\frac{\partial u_z}{\partial r}\tag{4}$$

The constitutive relations for FGMs are similar to the relations of isotropic materials except that the stiffnesses are functions of radial coordinate because material properties E and ν distributed according to the power law distribution. The constitutive relations are stated as:

$$\begin{Bmatrix}\sigma_z\\ \sigma_\theta\\ \sigma_r\end{Bmatrix}=\begin{bmatrix}C_{11}&C_{12}&C_{12}\\ C_{12}&C_{11}&C_{12}\\ C_{12}&C_{12}&C_{11}\end{bmatrix}\begin{Bmatrix}\varepsilon_z\\ \varepsilon_\theta\\ \varepsilon_r\end{Bmatrix},\quad \sigma_{rz}=C_{66}\gamma_{rz}\tag{5}$$

where

$$C_{11}=\frac{E(1-\nu)}{(1+\nu)(1-2\nu)},\quad C_{12}=\frac{E\nu}{(1+\nu)(1-2\nu)},\quad C_{66}=\frac{C_{11}-C_{12}}{2}\tag{6}$$

Upon substitution of Eqs. (4) into Eqs. (5), the constitutive relations can be rewritten as follows:

$$\begin{aligned}\sigma_z&=C_{11}\frac{\partial u_z}{\partial z}+C_{12}\left(\frac{u_r}{r}+\frac{\partial u_r}{\partial r}\right)\\ \sigma_\theta&=C_{11}\frac{u_r}{r}+C_{12}\left(\frac{\partial u_z}{\partial z}+\frac{\partial u_r}{\partial r}\right)\\ \sigma_r&=C_{11}\frac{\partial u_r}{\partial r}+C_{12}\left(\frac{u_r}{r}+\frac{\partial u_z}{\partial z}\right)\\ \sigma_{rz}&=C_{66}\left(\frac{\partial u_r}{\partial z}+\frac{\partial u_z}{\partial r}\right)\end{aligned}\tag{7}$$

Lastly, substituting Eqs. (7) into Eqs. (3) yields the governing (i.e., displacement) equations of motion:

$$\begin{aligned}&\frac{1}{r}\frac{\partial}{\partial r}\left[C_{11}r\frac{\partial u_r}{\partial r}+C_{12}\left(u_r+r\frac{\partial u_z}{\partial z}\right)\right]+\frac{\partial}{\partial z}\left[C_{66}\left(\frac{\partial u_z}{\partial r}+\frac{\partial u_r}{\partial z}\right)\right]\\&\quad-C_{11}\frac{u_r}{r^2}-\frac{C_{12}}{r}\left(\frac{\partial u_r}{\partial r}+\frac{\partial u_z}{\partial z}\right)=\rho\frac{\partial^2 u_r}{\partial t^2}\\&\frac{\partial}{\partial z}\left[C_{11}\frac{\partial u_z}{\partial z}+C_{12}\left(\frac{u_r}{r}+\frac{\partial u_r}{\partial r}\right)\right]+\frac{1}{r}\frac{\partial}{\partial r}\left[C_{66}r\left(\frac{\partial u_z}{\partial r}+\frac{\partial u_r}{\partial z}\right)\right]=\rho\frac{\partial^2 u_z}{\partial t^2}\end{aligned}\tag{8}$$

where Eqs. (8) are known as the Navier equations of motion.

3. Finite Element Formulation

For functionally graded materials, the material properties are complex function of

position r, and the Navier equations in (8) are not amenable to analytical solutions. Here, a two-dimensional finite element method is used to solve Eqs. (8). To this end, an especial element is developed to consider exactly the material distribution through the thickness of the FGM cylinder.

By applying the Rayleigh-Ritz technique to the system of Navier equations in (8), weak formulations are obtained as:

$$\int\left\{\frac{\partial w_1}{\partial r}\left[C_{11}r\frac{\partial u_r}{\partial r}+C_{12}\left(u_r+r\frac{\partial u_z}{\partial z}\right)\right]+\frac{\partial w_1}{\partial z}\left[C_{66}r\left(\frac{\partial u_z}{\partial r}+\frac{\partial u_r}{\partial z}\right)\right]\right.$$
$$\left.+w_1\left[C_{11}\frac{u_r}{r}+C_{12}\left(\frac{\partial u_z}{\partial z}+\frac{\partial u_r}{\partial r}\right)\right]+\rho r w_1\ddot{u}_r\right\}drdz-\oint w_1\tau_r\,ds=0$$
$$\int\left\{\frac{\partial w_2}{\partial z}\left[C_{11}r\frac{\partial u_z}{\partial z}+C_{12}\left(u_r+r\frac{\partial u_r}{\partial r}\right)\right]\right. \tag{9}$$
$$\left.+\frac{\partial w_2}{\partial r}\left[C_{66}r\left(\frac{\partial u_z}{\partial r}+\frac{\partial u_r}{\partial z}\right)\right]+\rho r w_2\ddot{u}_z\right\}drdz-\oint w_2\tau_z\,ds=0$$

where w_1 and w_2 are weight functions and τ_r and τ_z are the force tractions on the boundary of the cylinder, which are defined as:

$$\tau_r=\sigma_r l_r+\sigma_{rz}l_z$$
$$\tau_z=\sigma_z l_z+\sigma_{rz}l_r \tag{10}$$

In Eqs. (9) the dot represents the derivative with respect to time. Next, let a section of the cylinder be divided into a finite number of elements interconnected only at nodal points. The rectangular elements have two degrees of freedom in each node and they are placed in the radial and longitudinal directions of the cylinder as shown in Fig. 3. Also, the linear interpolation functions are selected as:

$$\psi_1=\left(1-\frac{r}{a}\right)\left(1-\frac{z}{b}\right),\quad \psi_2=\frac{r}{a}\left(1-\frac{z}{b}\right),\quad \psi_3=\frac{z}{b}\left(1-\frac{r}{a}\right),\quad \psi_4=\frac{z}{b}\frac{r}{a} \tag{11}$$

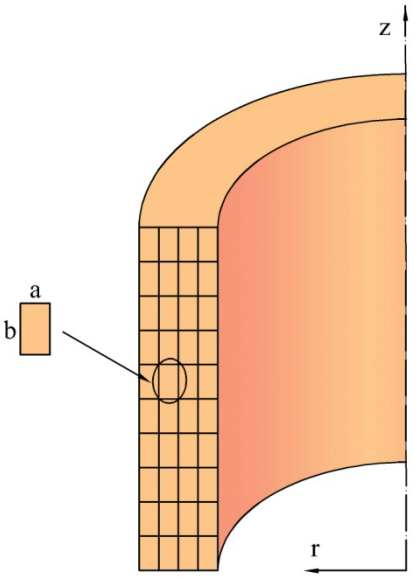

Figure 3. Arrangement of elements in the cylinder cross-section.

Displacements are approximated with summation of interpolation functions as:

$$u_r = \sum_{j=1}^{n_e} u_j \psi_j, \quad u_z = \sum_{j=1}^{n_e} v_j \psi_j \tag{12}$$

Next, the weight functions are replaced by the interpolation functions to obtain the following weak forms:

$$\int \left\{ C_{11} r \frac{\partial \psi_i}{\partial r} \frac{\partial \psi_j}{\partial r} u_j + C_{12} \frac{\partial \psi_i}{\partial r} \psi_j u_j + C_{12} r \frac{\partial \psi_i}{\partial r} \frac{\partial \psi_j}{\partial z} v_j + C_{12} \frac{\partial \psi_j}{\partial z} \psi_i v_j + C_{66} r \frac{\partial \psi_i}{\partial z} \frac{\partial \psi_j}{\partial z} u_j \right.$$
$$\left. + C_{66} r \frac{\partial \psi_i}{\partial z} \frac{\partial \psi_j}{\partial r} v_j + \frac{C_{11}}{r} \psi_i \psi_j u_j + C_{12} \frac{\partial \psi_j}{\partial r} \psi_i u_j + \rho r \psi_i \psi_j \ddot{u}_j \right\} dr dz = \oint \psi_i \tau_r$$
$$\int \left\{ C_{66} r \frac{\partial \psi_i}{\partial r} \frac{\partial \psi_j}{\partial r} v_j + C_{66} r \frac{\partial \psi_i}{\partial r} \frac{\partial \psi_j}{\partial z} u_j + C_{11} r \frac{\partial \psi_i}{\partial z} \frac{\partial \psi_j}{\partial z} v_j + C_{12} \frac{\partial \psi_i}{\partial z} \psi_j u_j \right.$$
$$\left. + C_{12} r \frac{\partial \psi_i}{\partial z} \frac{\partial \psi_j}{\partial r} u_j + \rho r \psi_i \psi_j \ddot{v}_j \right\} dr dz = \oint \psi_i \tau_z \, ds \tag{13}$$

Eqs. (13) can be written in matrix form as:

$$\begin{bmatrix} [M^{11}] & [0] \\ [0] & [M^{22}] \end{bmatrix} \begin{Bmatrix} \{\ddot{u}\} \\ \{\ddot{v}\} \end{Bmatrix} + \begin{bmatrix} [K^{11}] & [K^{12}] \\ [K^{21}] & [K^{22}] \end{bmatrix} \begin{Bmatrix} \{u\} \\ \{v\} \end{Bmatrix} = \begin{Bmatrix} \{F^1\} \\ \{F^2\} \end{Bmatrix} \tag{14}$$

or

$$[M^e]\{\ddot{U}^e\} + [K^e]\{U^e\} = \{F^e\} \tag{15}$$

where U denotes the displacement components and index e expresses parameters over each element. The components of mass, stiffness and force matrices of especial FGM element are defined as:

$$M_{ij}^{11} = M_{ij}^{22} = \int \rho \psi_i \psi_j \, r dr dz$$

$$K_{ij}^{11} = \int \left\{ C_{11} r \frac{\partial \psi_i}{\partial r} \frac{\partial \psi_j}{\partial r} + C_{12} \frac{\partial \psi_i}{\partial r} \psi_j + \frac{C_{11}}{r} \psi_i \psi_j + C_{12} \frac{\partial \psi_j}{\partial r} \psi_i + C_{66} r \frac{\partial \psi_i}{\partial z} \frac{\partial \psi_j}{\partial z} \right\} dr dz$$

$$K_{ij}^{12} = K_{ji}^{21} = \int \left\{ C_{12} r \frac{\partial \psi_i}{\partial r} \frac{\partial \psi_j}{\partial z} + C_{12} \psi_i \frac{\partial \psi_j}{\partial z} + C_{66} r \frac{\partial \psi_i}{\partial z} \frac{\partial \psi_j}{\partial r} \right\} dr dz \tag{16}$$

$$K_{ij}^{22} = \int \left\{ C_{66} r \frac{\partial \psi_i}{\partial r} \frac{\partial \psi_j}{\partial r} + C_{11} r \frac{\partial \psi_i}{\partial z} \frac{\partial \psi_j}{\partial z} \right\} dr dz$$

$$F_i^1 = \oint \psi_i t_r \, ds$$

$$F_i^2 = \oint \psi_i t_z \, ds$$

The matrices $[K^e]$ and $[M^e]$ are calculated for each individual element and then through an assemblage process the global assembled matrixes $[K]$ and $[M]$ for the whole FGM cylinder are calculated. The global form of Eq. (15) can be writhen as:

$$[M]\{\ddot{U}\} + [K]\{U\} = \{F\} \tag{17}$$

In this study, all of the integrations in Eqs. (16) are calculated analytically over each element domain to avoid any numerical errors.

Once the finite element equations of motion are established, different numerical methods can be employed to solve them in space and time domains. In the case of transient

response, Eq. (17) must be integrated with respect to time t to determine the nodal values as functions of time. The Newmark direct integration method with suitable time step that is used widely in structural dynamics is employed and the equations of motion are solved (see, for example, Ref. (18) about the details on method).

4. Results and Discussion

In this study, a finite element code is developed in the programming environment of MATLAB®. To demonstrate the validity and applicability of the numerical procedure, some simple examples will be discussed.

Primarily, by increasing the number of elements in the radial and axial directions, convergence of the results is studied. Here a FGM cylinder subjected to a constant internal pressure is used for convergence study to find the number of elements required for analyses. The cylinder is assumed to have the ratios of the inner and outer radiuses to thickness of $r_{in}/h=1$ and $r_{out}/h=2$ and the length of 1 m. In this case, the present results are obtained with various number of elements in the radial and axial directions. It is observed that with five elements in the radial direction and twenty elements in the axial direction, the results converge with a very good degree of accuracy. To this end, the cylinders are divided into, unless otherwise mentioned, five and twenty elements in the radial and axial directions, respectively, in the subsequent calculations. It is once again mentioned here that, in this study, there are no domain approximation and numerical errors because the domain is rectangular and all of the elements are rectangular as well and also all of the integrations in Eqs. (16) are calculated analytically.

The accuracy and effectiveness of the present method are demonstrated by comparing the results of the present method with the results of hybrid numerical method (HNM) presented by Ref. (2), which had combined the finite element method with the Fourier transformation method. In the HNM, the FGM cylinder is divided into N cylindrical elements with three-nodal line in the wall thickness and the element material properties are assumed to vary linearly in the thickness direction for enhanced modeling of the spatial variation of material properties in FGM. The thick FGM cylinder (r_{in}=h) with Silicon nitride on its inner surface and Stainless steel on its outer surface with the power law exponent n=4 is considered. The material properties of Silicon nitride and Stainless steel are shown in Table 1. The cylinder is subjected to radial line load which uniformly distributed along the circumferential direction. In the calculations, the following dimensionless parameters are used (see Ref. (2)):

$$c_s=\sqrt{\frac{C_{66}}{\rho_c}},\quad \bar{t}=\frac{tc_s}{h},\quad \bar{u}_r=\frac{C_{66}u_r}{r_{out}} \tag{18}$$

where C_{66} and ρ_c stand for reference material constant and mass density. Here, they are equal to the material constant C_{66} and mass density on the inner surface of the cylinder under consideration.

The radial incident wavelet is assumed to be a radial line load acting on the outer surface of the cylinder. The loading function is defined as:

$$f(t)=\begin{cases}\sin(2\pi t/T_{wa}) & 0<t<T_{wa}\\ 0 & t\le 0 \text{ and } t\ge T_{wa}\end{cases} \tag{19}$$

where T_{wa} is the time duration of radial incident wavelet and we set $\bar{T}_{wa}=2$. It means that the wavelet is one cycle of the sine function.

Time history of the radial displacement at $z=10h$ on the outer surface of the cylinder excited at z = 0, is shown in Fig. 4. It is seen that there is a good agreement between the present solution and that of Ref. (2). Specifically, the maximum radial deflections obtained

by the two methods are approximately identical and, therefore, the present method can be used to obtain dynamic load factor. Also, the averages of time periods are derivable from Fig. 4. It is found that the normalized time period of the result of Ref. (2) is about 1.5 but the normalized time period of the present result is about 2.3 which is closer to the time duration of radial incident wavelet $\overline{T}_{wa}=2$. It is inferred that the reason of this difference is through the distinction in method of solutions. Ref. (2) used Fourier transformations to obtain the transient response but we used the Newmark direct integration method for solving the equations of motion.

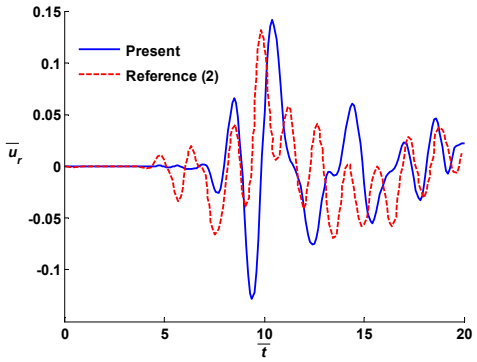

Figure 4. Time history of the radial displacement at z=10h on the outer surface of the thick cylinder.

To illustrate dynamic response of the functionally graded cylinders, loads are applied to the cylinder in radial directions which distributed as internal pressure or concentrated as radial line load. Also, load exerted to the cylinder from zero to final value in two different manners. First, load increases as a sine function. Next, load is applied suddenly. These loads are uniformly distributed along circumferential direction. In all of the loadings, time history diagrams are presented and from which dynamic load factors are calculated and tabulated for pure and functionally graded cylinders.

The functionally graded cylinder is assumed to be made of a combination of metal (Ti–6Al–4V) and ceramic (ZrO_2) with the material properties shown in Table 1. The effects of FGM configuration are studied by considering the responses of two FGM cylinders: Type 1 and Type 2. The former has metal on its outer surface and ceramic on its inner surface, while the latter is reverse. For both types of cylinders, power law exponent n=1 is considered.

Table 1. Material properties of metals and ceramics (see Refs. (2) and (19)).

Stainless steel	Silicon nitride	Ti–6Al–4V	ZrO2
$E=207.8$ GPa	$E=322.4$ GPa	$E=66.2$ GPa	$E=117.0$ GPa
$\nu=0.317$	$\nu=0.24$	$\nu=0.321$	$\nu=0.333$
$\rho=8.17\times10^3$ kg/m^3	$\rho=2.37\times10^3$ kg/m^3	$\rho=4.41\times10^3$ kg/m^3	$\rho=5.6\times10^3$ kg/m^3

Next, two ratios of the inner radius to thickness, are employed in calculations; the cylinder with $r_{in}/h=1$ is viewed as a thick cylinder, and with $r_{in}/h=20$ is viewed as a cylindrical shell. Also, it is assumed that the cylinders have clamped boundary conditions at the ends and the ratios of the length to inner radius are considered as $L/r_{in}=20$. In all of the following computations these assumptions and parameters are used.

4.1 Increasingly Loading

Suppose that the load increases from zero to its final value by the following sine

function equation:

$$f(t)=\begin{cases} P_0 \sin(2\pi t/T) & 0<t<T/4 \\ P_0 & t\geq T/4 \end{cases} \tag{20}$$

where P_0 indicates the numerical value of the final load. For the case of internal pressure loading, it is assumed that P_0=100 kPa and for the case of radial line loading, it is assumed that P_0=-10^4 N/m. Also, T denotes the time duration of sine function. Therefore, loads are increasing to final value in quarter time duration T. In order to study the response of the cylinders to abrupt dynamic loadings, it is essential to select a proper value for time duration T. Here, separate values are selected for cylindrical shell and thick cylinder. The reason of the difference between these values is that the natural frequencies of the thick cylinder are greater than those of the cylindrical shell. Fig. 5 shows the variation of internal pressure with respect to time.

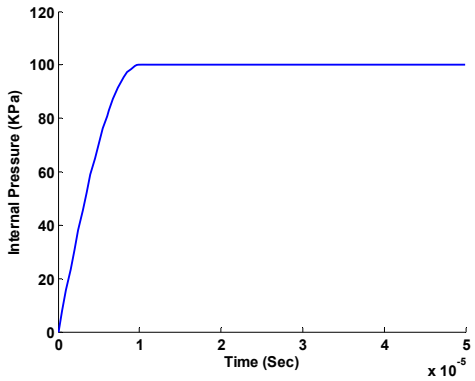

Figure 5. Variation of internal pressure in increasingly loading condition for $T=4\times10^{-5}$s .

Here, it is assuming that $T=4\times10^{-4}$s for the cylindrical shell and $T=4\times10^{-5}$s for the thick cylinder. The time histories of the radial displacement at the middle length on the outer surface of the cylinders are shown in Fig. 6 for internal pressure loading and in Fig. 7 for radial line loading. It is noted that, in the case of radial line loading, since the applied load is compressive, the radial displacements are negative in the figures. It is seen that the time history response of the radial displacement of FGM cylinders is between the response of metal and ceramic cylinders. Dynamic load factor is calculated by dividing the maximum value of the radial displacement in dynamic loading condition to the maximum value of the radial displacement in static loading condition [20]. Therefore, from results of dynamic loading and by calculating the radial displacement of cylinders under static loading, dynamic load factors are calculated for three values of T and displayed in Table 2. These values reveal that dynamic load factor for metal cylinder is greater than that of ceramic cylinder as expected. It is also seen that the values of dynamic load factor for FGM cylinder are between the values of metal and ceramic cylinders.

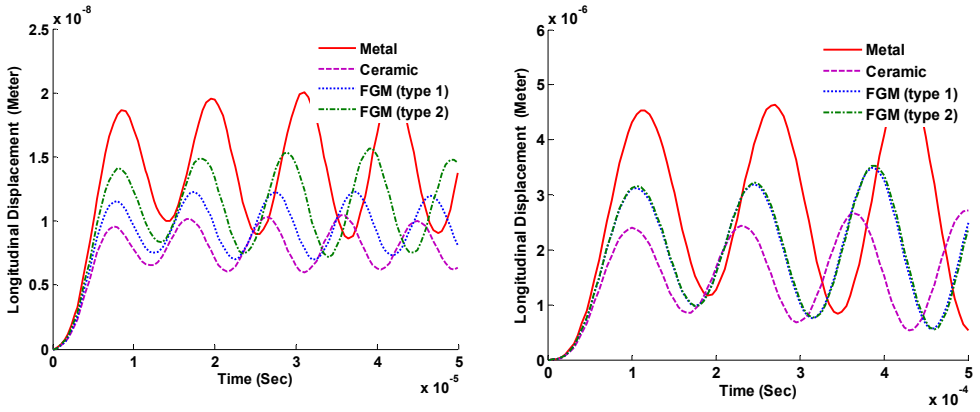

(a) (b)

Figure 6. Time history of the radial displacement in the (a) thick cylinder and (b) cylindrical shell subjected to increasingly internal pressure loading.

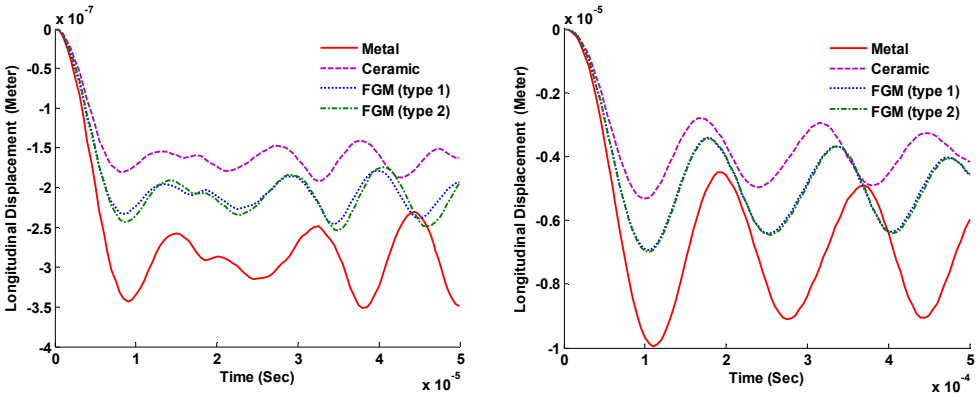

(a) (b)

Figure 7. Time history of the radial displacement in the (a) thick cylinder and (b) cylindrical shell subjected to increasingly radial line loading.

Table 2. Values of dynamic load factor in the case of increasing loading.

Loading	Cylinder	Thick cylinder			Cylindrical shell		
		$T\times10^5$			$T\times10^4$		
		2	3	4	2	3	4
Internal pressure loading	Metal	1.6803	1.4857	1.2934	1.8699	1.7425	1.5882
	Ceramic	1.6124	1.3788	1.1667	1.8276	1.6587	1.4790
	FGM (type 1)	1.6410	1.4056	1.1972	1.8443	1.6932	1.5238
	FGM (type 2)	1.6517	1.4426	1.2398	1.8458	1.6943	1.5268
Radial line loading	Metal	1.4180	1.3025	1.1823	1.6146	1.5320	1.4273
	Ceramic	1.3756	1.2374	1.0928	1.5885	1.4783	1.3451
	FGM (type 1)	1.3789	1.2443	1.1113	1.6006	1.5007	1.3780
	FGM (type 2)	1.4073	1.2809	1.1484	1.6014	1.5025	1.3808

4.2 Suddenly Loading

Consider load P_0 with the numerical values of the previous examples is applied suddenly (i.e., step excitation) to the cylinders for both cases of the internal pressure and radial line loading.

The time histories of the radial displacement at the middle length on the outer surface

of the cylinders are shown in Fig. 8 for internal pressure loading and in Fig. 9 for radial line loading. Also, the dynamic load factors for this loading case are displayed in Table 3. It is seen that dynamic load factors for suddenly internal pressure loading are greater than those of the previous loading and they are approximately equal to 2 as predicted in the literature. It is also revealed that even in suddenly loading, dynamic behavior of FGM cylinders is similar to the behavior of pure cylinders.

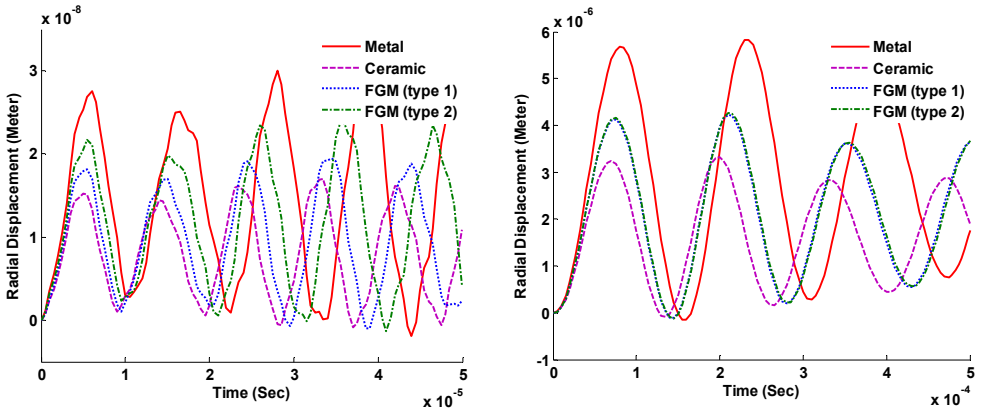

(a) (b)

Figure 8. Time history of the radial displacement in the (a) thick cylinder and (b) cylindrical shell subjected to suddenly internal pressure loading.

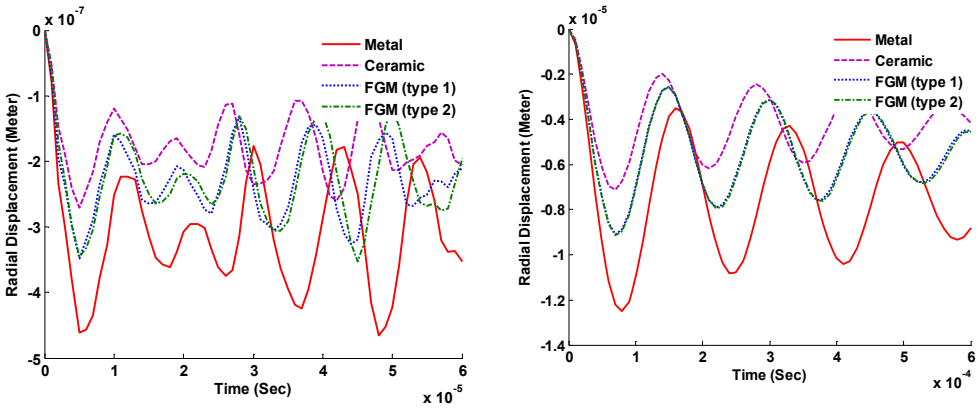

(a) (b)

Figure 9. Time history of the radial displacement in the (a) thick cylinder and (b) cylindrical shell subjected to suddenly radial line loading.

Table 3. Values of dynamic load factor in the case of suddenly loading.

Loading	Cylinder	Thick cylinder	Cylindrical shell
Internal pressure loading	Metal	1.9145	1.9865
	Ceramic	1.8640	1.9837
	FGM (type 1)	1.8835	1.9833
	FGM (type 2)	1.9037	1.9839
Radial line loading	Metal	1.4776	1.6787
	Ceramic	1.5159	1.6758
	FGM (type 1)	1.5064	1.6777
	FGM (type 2)	1.5157	1.6765

4.5 Effects of Power Law Exponent *n*

Here, the effects of variation of power low exponent *n* on dynamic load factor are

investigated. To this purpose, type 1 of FGM cylinders with various power law exponent n are subjected to suddenly internal pressure as previous sections. Time histories of the radial displacement at the middle length on the outer surface of the cylinders are displayed in Fig. 10. It is seen that with increasing the power law exponent n maximum deflection is decreased, as expected, because the portion of ceramic in cylinders is increased. Also, for these loading cases, dynamic load factors for wide range of the power law exponent n are calculated and plotted in semi logarithmic diagrams which illustrated in Fig. 11. It is observed that with increasing the power law exponent n dynamic load factor is approximately decreased.

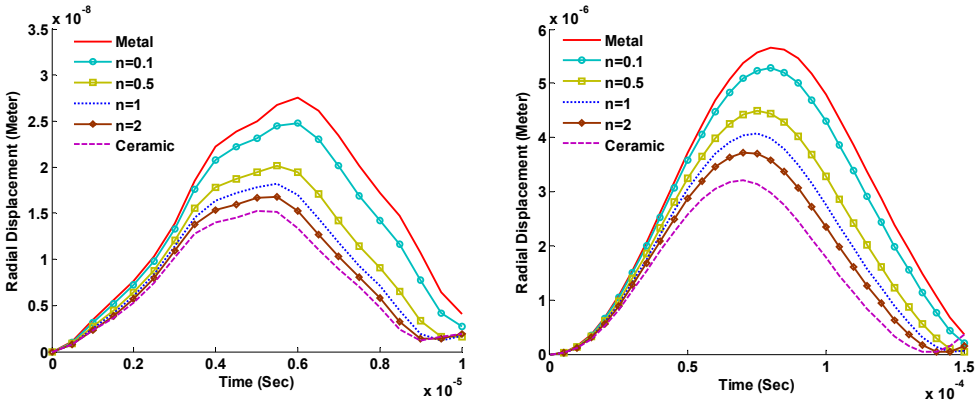

(a) (b)

Figure 10. Time history of the radial displacement in the (a) thick cylinder and (b) cylindrical shell subjected to suddenly internal pressure loading.

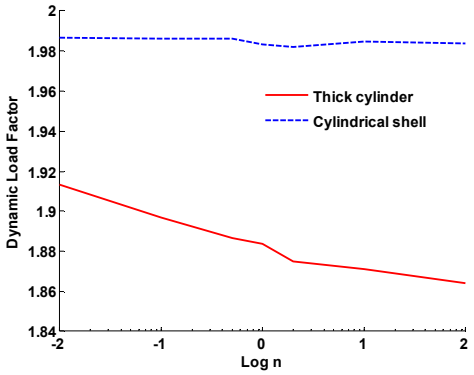

Figure 11. Variation of dynamic load factor for wide range of the power law exponent n in the FGM cylinders subjected to suddenly internal pressure loading.

5. Conclusions

Analysis of functionally graded hollow cylinders with finite length under axisymmetric dynamic loads is presented. Two-dimensional finite element and the Newmark methods are used for solving governing equations of motion. For increasing accuracy of the solution, an especial element is introduced in which material properties can be considered variable inside the element exactly according to the distribution of material properties in FGM cylinders. Two types of dynamic loads are applied and the results are compared. Numerical results reveal that dynamic responses of FGM cylinders are between the responses of metal and ceramic cylinders. It is also found that the dynamic load factors of FGM cylinders are close to those of pure cylinders.

References

(1) Gong, S.W., Lam, K.Y. and Reddy, J.N., Elastic Response of Functionally Graded Cylindrical Shells to Low-Velocity Impact, *International Journal of Impact Engineering*, Vol.22, No.4 (1999), pp.397-417.

(2) Han, X., Liu, G.R., Xi, Z.C. and Lam, K.Y., Transient Waves in a Functionally Graded Cylinder, *International Journal of Solids and Structures*, Vol.38, No.17 (2001), pp.3021-3037.

(3) Nelson, R.B., Dong, S.B. and Kalra, R.D., Vibrations and Waves in Laminated Orthotropic Circular Cylinders, *Journal of Sound and Vibration*, Vol.18, No.3 (1971), pp.429-444.

(4) Han, X., Liu, G.R., Xi, Z.C. and Lam, K.Y., Characteristics of Waves in a Functionally Graded Cylinder, *International Journal for Numerical Methods in Engineering*, Vol.53, No.3 (2002), pp.653-676.

(5) Han, X., Xu, D. and Liu, G.R., Transient Responses in a Functionally Graded Cylindrical Shell to a Point Load, *Journal of Sound and Vibration*, Vol.251, No.5 (2002), pp.783-805.

(6) Elmaimouni, L., Lefebvre, J.E., Zhang, V. and Gryba, T., Guided Waves in Radially Graded Cylinders: A Polynomial Approach, *NDT & E International*, Vol.38, No.5 (2005), pp.344-353.

(7) Shakeri, M., Akhlaghi, M. and Hoseini, S.M., Vibration and Radial Wave Propagation Velocity in Functionally Graded Thick Hollow Cylinder, *Composite Structures*, Vol.76, No.1-2 (2006), pp.174-181.

(8) Asgari, M., Akhlaghi, M. and Hosseini, S.M., Dynamic Analysis of Two-Dimensional Functionally Graded Thick Hollow Cylinder with Finite Length under Impact Loading, *Acta Mechanica*, Vol.208, No.3-4 (2009), pp.163-180.

(9) Loy, C.T., Lam, K.Y. and Reddy, J.N., Vibration of Functionally Graded Cylindrical Shells, *International Journal of Mechanical Sciences*, Vol.41, No.3 (1999), pp.309-324.

(10) Pradhan, S.C., Loy, C.T., Lam, K.Y. and Reddy, J.N., Vibration Characteristics of Functionally Graded Cylindrical Shells under Various Boundary Conditions, *Applied Acoustics*, Vol.61, No.1 (2000), pp.111-129.

(11) Yang, J. and Shen, H.S., Free Vibration and Parametric Resonance of Shear Deformable Functionally Graded Cylindrical Panels, *Journal of Sound and Vibration*, Vol.261, No.5 (2003), pp.871-893.

(12) Najafizadeh, M.M. and Isvandzibaei, M.R., Vibration of Functionally Graded Cylindrical Shells based on Higher Order Shear Deformation Plate Theory with Ring Support, *Acta Mechanica*, Vol.191, No.1-2 (2007), pp.75-91.

(13) Ansari, R. and Darvizeh, M., Prediction of Dynamic Behaviour of FGM Shells under Arbitrary Boundary Conditions, *Composite Structures*, Vol.85, No.4 (2008), pp.284-292.

(14) Sofiyev, A.H., Dynamic Buckling of Functionally Graded Cylindrical Thin Shells under Non-Periodic Impulsive Loading, *Acta Mechanica*, Vol.165, No.3-4 (2003), pp.151-163.

(15) Sofiyev, A.H., The Stability of Functionally Graded Truncated Conical Shells subjected to a Periodic Impulsive Loading, *International Journal of Solids and Structures*, Vol.41, No.13 (2004), pp.3411-3424.

(16) Sofiyev, A.H., The Stability of Compositionally Graded Ceramic-Metal Cylindrical Shells under a Periodic Axial Impulsive Loading, *Composite Structures*, Vol.69, No.2 (2005), pp.247-257.

(17) Kadoli, R. and Ganesan, N., Buckling and Free Vibration Analysis of Functionally Graded Cylindrical Shells subjected to a Temperature-Specified Boundary Condition, *Journal of Sound and Vibration*, Vol.289, No.3 (2006), pp.450-480.

(18) Reddy, J.N., *Energy Principles and Variational Methods in Applied Mechanics*, (2002), John Wiley & Sons.

(19) Bahtui, A. and Eslami, M.R., Coupled Thermoelasticity of Functionally Graded Cylindrical Shells, *Mechanics Research Communications*, Vol.34, No.1 (2007), pp.1-18.

(20) Ashebo, D.B., Chan, T.H.T. and Yu, L., Evaluation of Dynamic Loads on a Skew Box Girder Continuous Bridge Part II: Parametric Study and Dynamic Load Factor, *Engineering Structures*, Vol.29, No.6 (2007), pp.1064-1073.